

R. Qiao

Effects of molecular level surface roughness on electroosmotic flow

Received: 24 March 2006 / Accepted: 15 May 2006 / Published online: 30 June 2006
© Springer-Verlag 2006

Abstract Electroosmotic flow is widely used to transport and mix fluids in micro- and nanofluidic systems. Though essentially all surfaces exhibit certain degrees of roughness, the effects of surface roughness on electroosmotic flow is not well-understood. In this paper, we investigate how the electrical double layer and electroosmotic flow are affected by molecular level surface roughness by using molecular dynamics simulations. The simulation results indicate that, when the thickness of the electrical double layer is comparable to the height of surface roughness, presence of sub-nanometer deep concave regions on a rough surface can alter the electrical double layer near the surface, and reduce the electroosmotic flow significantly.

Keywords Electroosmotic flow · Electrical double layer · Microfluidics · Nanofluidics · Surface roughness

1 Introduction

When an electrolyte solution is in contact with a charged surface, an electrical double layer (EDL) with non-zero charge density will develop near the surface. If an external electric field is applied parallel to the surface, the fluid will be driven by the excess counter-ions in the EDL, and electroosmotic flow is obtained. Because of its excellent scalability, low dispersion and easy-of-control (Probstein 1994), electroosmotic flow has become one of the most important fluid transport method used in micro- and nanofluidic systems (Harrison et al. 1993; Yang and Li 1997; Kemery et al. 1998; Kuo et al. 2001; Santiago 2001).

Surface roughness is a ubiquitous phenomenon, and most surfaces have certain degree of roughness either incurred during fabrication process or due to the

adsorption of other species such as macromolecules. Though atomically smooth surface does exist [e.g., fresh silica capillary surface (Watzig et al. 2003)], the surface of micro- and nanofluidic channels typically has a roughness of a few angstroms to a few micrometers (Watzig et al. 2003; Qu et al. 2000). While it is known that electroosmotic flow is sensitive to the surface properties (Lyklema 1995), the effects of surface roughness on electroosmotic flow received only scant attention in the past. The first systematic study is perhaps due to Dukhin and Derjaguin (1974), who identified two critical length scales of the problem, i.e., the thickness of electrical double layer (typically characterized by the Debye length (Lyklema 1995)) and the characteristic length scale of the surface roughness. When the EDL thickness is much smaller compared to the surface roughness, the electroosmotic flow near the concave portion of the rough surface is essentially the same as that near a smooth surface, and the Smoluchowski equation is valid. The electroosmotic flow at position away from the rough surface can then be calculated by using the standard models (Probstein 1994). When the EDL thickness is much greater than the surface roughness, the electroosmotic velocity can again be described by the Smoluchowski equation. However, in such a case, the effective charge density of the rough surface is higher than the corresponding smooth surface due to the increased area of the rough surface. Most recently, Hu et al. (2003) studied the effect of surface roughness on the electroosmotic flow in microchannels at the thin EDL limit. Their study indicates that the electroosmotic flow in microchannels can be significantly reduced by surface roughness, and high pressure can be induced in the channels.

While these prior studies have improved our understanding of the surface roughness effect on the electroosmotic flow, several important aspects of the problem were not addressed. First, the scenario where the Debye length is comparable to surface roughness is seldom studied. Such a scenario usually arises when the electrolyte is at physiological concentrations ($c \approx 0.15$ M,

R. Qiao
Department of Mechanical Engineering,
Clemson University, Clemson, SC 29634, USA
E-mail: rqiao@clemson.edu
URL: <http://www.clemson.edu/~rqiao>

Debye length $\lambda_D = 8 \text{ \AA}$) or in closed nanofluidic system with moderate to high surface charge density where the effective Debye length can be small (Tessier and Slater 2006). Second, in most studies, the electrical double layer is modeled by the Poisson–Boltzmann equation, whose accuracy can be in question for thin EDL as the molecular nature of ion, water and surfaces and the discreteness of surface charges are not accounted in its formulation (Qiao and Aluru 2003).

In this paper, we study the effects of surface roughness on EDL and electroosmotic flow by using molecular dynamics (MD) simulations. We limit our study to the situation where both the surface roughness and the Debye length is at the molecular (i.e., sub-nanometer) level. Specifically, we investigate how the water density, ion distribution and electroosmotic velocity are affected by the nanometer wide and sub-nanometer deep rough spots on the surface. The paper is organized as follows: Section 2 describes the set up of the simulation system and MD simulation details, Sect. 3 presents the simulation results and discussion. Finally, conclusions are presented in Sect. 4.

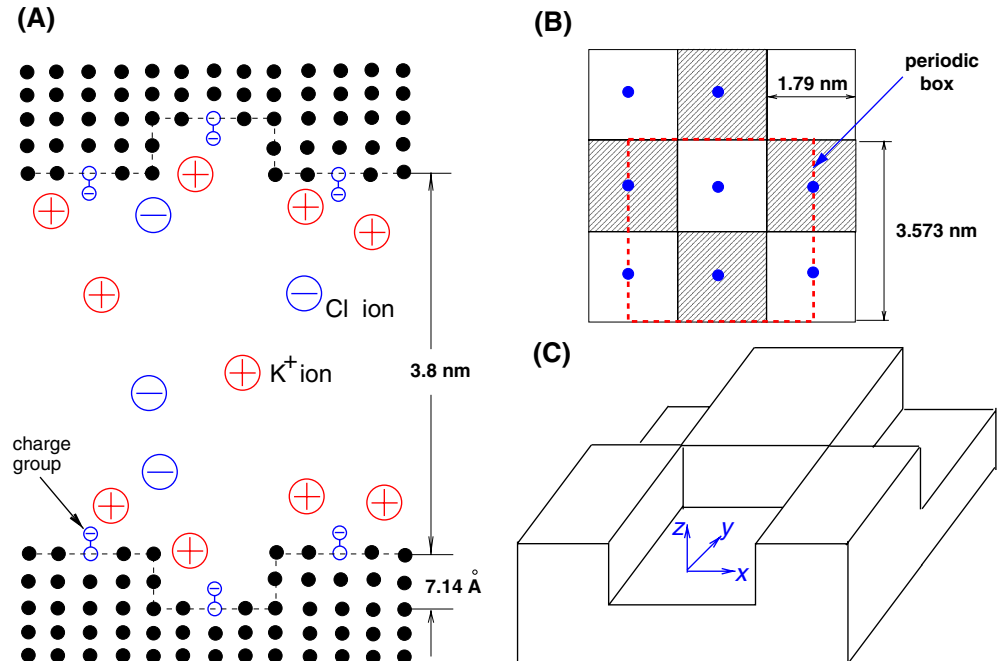
2 Simulation setup and methods

Figure 1 shows the setup of the simulation systems. Two simulation systems were investigated in this paper. Both systems consist of a slab of KCl solution enclosed by two channel walls. In the first case, a smooth channel wall is implemented. The smooth channel wall has a lateral dimension of $3.573 \times 3.573 \text{ nm}^2$, and consists of six layers of atoms arranged in a cubic lattice. Each wall atom is tethered to its lattice by a spring. The channel

width, measured as the distance between the two innermost layers of the upper and lower channel wall, is 3.8 nm . Such a width is large enough to observe bulk-like behavior in the channel center region (Qiao and Aluru 2003). Four charge groups, each consisting of one neutral wall atom and one oxygen atom carrying $-e$ charge, were anchored evenly to the top layer of each channel wall to produce a surface charge density of -0.05 C/m^2 . In the second system, a rough channel wall is adopted. The rough wall is constructed by removing two blocks of surface atoms from the smooth channel wall (see Fig. 1b, c). The square-shaped concave spots of the rough surface has a depth of 7.14 \AA , and a cross-sectional area of $1.79 \times 1.79 \text{ nm}^2$. Note that there could be surface charge on the side wall in practical systems. However, in this initial study, we choose not to put charge on the side walls since this allows us to isolate the effects of the physical roughness on the electrokinetic transport without the complication of increased effective surface charge density. In a more comprehensive study, it would be interesting to further explore how the increased effective surface charge would affect the flow by building upon the understanding obtained here. The width of the rough channel is the same as that of the smooth channel. In both cases, the bulk concentration of the KCl solution, as measured by the K^+ and Cl^- ion concentration at the channel center, is $0.98 \pm 0.05 \text{ M}$, which corresponds to a Debye length of 3.07 \AA . There are 1,400 water molecules, 28 K^+ and 20 Cl^- ions in the first system, and 1,627 water molecules, 31 K^+ and 23 Cl^- ions in the second system.

Water is modeled by using the SPC/E model (Berendsen et al. 1987), and ions are modeled as charge Lennard–Jones atoms (Koneshan et al. 1998). The wall

Fig. 1 a A schematic of the system under investigation. The lateral dimension of the channel wall is $3.573 \times 3.573 \text{ nm}^2$. The water molecules enclosed in the channel are not shown for clarity. b A top-down view of the lower channel wall. The shaded regions denote the concave spots of the rough surface. The dots denote the charge groups. c A three dimensional view of the rough lower channel wall. Periodic boundary conditions are used in both x - and y -directions



atoms are modeled as Lennard–Jones spheres with force field parameters taken as the silicon atom in the Gromacs force field (Lindahl et al. 2001; Berendsen et al. 1995). Table 1 shows the force field parameters used in the simulation. The Lorentz–Berthelot combination rules are used to obtain the Lennard–Jones parameter for the pairs not shown in Table 1. Simulation were performed by using a modified Gromacs 3.0.5 (Lindahl et al. 2001; Berendsen et al. 1995). Periodic boundary conditions are used in the x - and y -directions. The electrostatic interactions were computed by using the slab PME method (Yeh and Berkowitz 1999). As required by the slab PME method, the length of the simulation box in z -direction is set as 12.1 nm. Other simulation details can be found in a prior publication (Qiao and Aluru 2003). A Nose thermostat (Nose 1984) was used to maintain the fluid and wall temperature at 300 K. To avoid biasing the velocity profile, only the velocity components in the direction orthogonal to the flow was thermostated. Because of the extremely high thermal noise, a strong electric field (0.24 V/nm) was applied in the x -direction in our simulations so that the fluid velocity can be retrieved with reasonable accuracy. It is important to note that using a strong electric field is a significant concern in MD simulations, and it is important to ensure that the system is in the linear response regime to avoid artifacts. Prior studies indicate that the flow response is linear up to a field of about 0.6 V/nm (Qiao and Aluru 2003), which is well beyond the present field strength. In addition, recent experiments indicated that the electric current response is linear even at 0.1 V/nm (Ho et al. 2005). So the results presented here should apply to the real laboratory situations. Even with such an electric field, the maximum water velocity in the simulations performed is 4.82 m/s, which is about 0.75% of the nominal thermal velocity of water at 300 K. The statistical uncertainties of the velocity profile are within 0.5 m/s (estimated by computing the standard deviation of the average velocity in channel using several simulations). Starting from a random configuration, each system is simulated for 2 ns to reach a steady state, and followed by a production run of 16 ns. The density and velocity profiles were obtained by using the binning method (Karniadakis et al. 2005).

3 Results and discussion

Figure 2a and b show the average water density and ion concentration profiles across the smooth channel. Because of the symmetry with respect to the channel center

Table 1 Parameters for the Lennard–Jones potential $U_{ij}(r) = 4\epsilon_{ij} \left[\left(\frac{\sigma_{ij}}{r} \right)^{12} - \left(\frac{\sigma_{ij}}{r} \right)^6 \right]$

Pair	σ (nm)	ϵ (kJ/mol)
Oxygen–Oxygen	0.3169	0.6502
K^+ – K^+	0.3331	0.4184
Cl^- – Cl^-	0.4401	0.4184
Wall–Wall	0.3386	2.4470

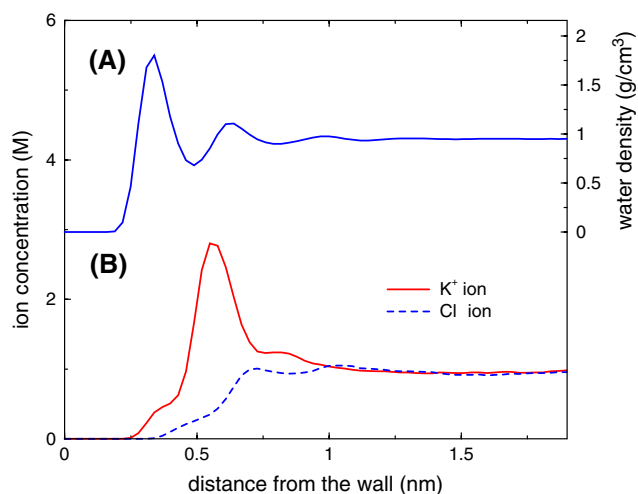


Fig. 2 **a** Water density distribution across the smooth channel. **b** K^+ and Cl^- ion concentration distribution across the smooth channel. The surface charge density is $-0.05 C/m^2$

line, only the density/concentration in the lower half of the channel is shown. Similar to most prior studies on fluid–solid interface (Karniadakis et al. 2005), a significant layering of water is observed near the solid wall. The oscillation of the water density penetrates about three water diameters into the fluids, and for $z > 1.0$ nm, the water density profile is essentially bulk-like. Though the K^+ ion concentration follows the general trend as expected from the Poisson–Boltzmann equation (Lyklema 1995), i.e., the counter-ion concentration decreases as we move away from the charged surface, it shows several interesting deviations. First, the K^+ ion concentration peak is not located at the closest approach distance ($z = 0.25$ nm) from the channel surface, but rather at $z = 0.55$ nm. Second, the K^+ ion concentration shows a weak plateau in the region $0.72 \text{ nm} < z < 0.85 \text{ nm}$. As explained in a prior publication (Qiao and Aluru 2005), both deviations originate from the ion hydration effect and are strongly correlated to the density oscillation of water near the solid wall, which are not accounted for in the Poisson–Boltzmann equation.

Figure 3 shows the electroosmotic velocity profile in the smooth channel. As expected, the velocity profile become essentially flat outside of the EDL ($z > 1.0$ nm). The ζ -potential of a charged surface is defined as (Lyklema 1995)

$$\zeta = -\frac{u_{eo}\eta}{\epsilon E_{ext}}, \quad (1)$$

where u_{eo} is the solvent velocity outside the EDL, and η and ϵ are the viscosity and permittivity of bulk electrolyte solution in contact with the charged surface, respectively. Since the EDL thickness is smaller compared to the channel width in our simulations, u_{eo} is taken as the water velocity in the channel center. Using a viscosity of 0.736 mPa and a permittivity of 7.17×10^{-11} F/m (Qiao and Aluru 2003), the ζ -potential of the smooth surface is computed to be -21.03 mV.

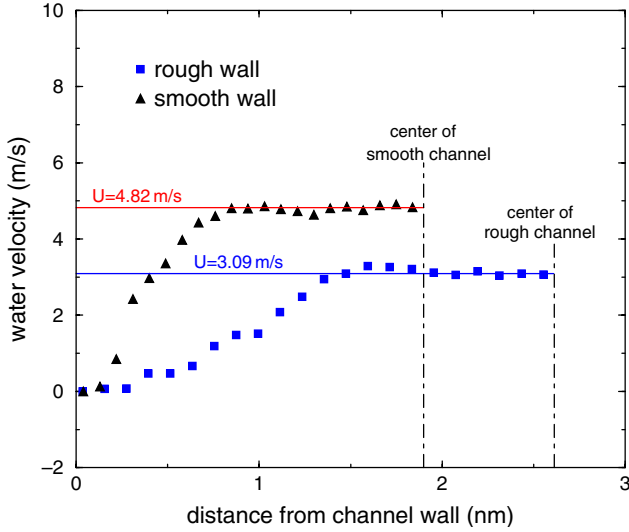


Fig. 3 Velocity profiles across the smooth and rough channels. The velocity profile is shown only for half of the channel due to the symmetry of the system with respect to the channel center line

The water and ion distribution is three dimensional when the surface is rough, which is difficult to visualize directly. We study the water and ion distribution using two approaches. In the first approach, we compute the one dimensional effective density/concentration profiles of water and ions across the rough channel. Specifically, the effective density/concentration is computed as the number of water/ion divided by the product of the total accessible area in the xy -plane and the thickness of sampling bin in the z -direction. The accessible area in the xy -plane, $A_{acc,xy}$ is defined as

$$A_{acc,xy} = \begin{cases} 3.573 \times 3.573 \text{ nm}^2 & \text{for } z > 0.714 \text{ nm} \\ (3.573/2 - \delta)^2 \times 2 \text{ nm}^2 & \text{for } z < 0.714 \text{ nm}, \end{cases} \quad (2)$$

where $\delta=0.16$ nm is the closest approach of water molecules towards the wall atoms. It is important to note that due to the discreteness of water molecule and the molecular size of the concave region, the accessible area cannot be defined unambiguously in the concave region (Travis 2000). Therefore, the effective density distribution provides mainly a convenient description of the location of the density peaks and the accessibility of water and ions to the concave region of the rough surface. In the second approach, we compute the water and ion concentration in the xz -plane passing through the charge group on the concave surface, which provides local details of the ion distribution near the charge group. These two approaches complement each other, and together provide us a detailed picture of the water and ion distribution in near the rough surface.

Figure 4a shows the effective density profiles of water across the rough channel. We observe two distinct peaks located at $z = 0.33$ and $z = 1.04$ nm, which corresponds to the layering of water near the concave and

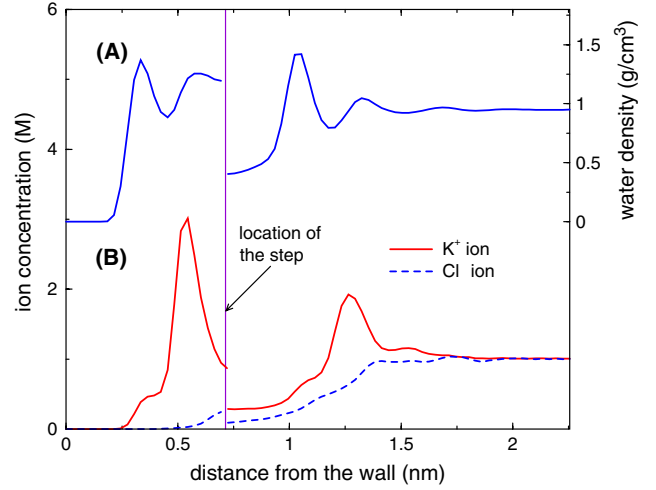


Fig. 4 **a** Effective water density (see text for definition) distribution across the rough channel surface. **b** Effective K^+ and Cl^- ion concentration distribution across the rough channel surface. The surface charge density is -0.05 C/m^2

convex surfaces of the rough surface, respectively. The first peak ($z = 0.33$ nm) clearly indicates that water penetrates into the nanometer wide and sub-nanometer deep concave spot on the rough surface. This is partially caused by the strongly attractive charge-dipole interactions between the charge group and water. The discontinuity of the density at $z = 0.714$ nm is caused by the fact that as we move across $z = 0.714$ nm, the accessible area in the xy -plane increase suddenly, but the number of water molecules in the xy -plane remains almost the same due to the exclusion of water by the convex surface of the wall. Figure 5 shows the water density distribution at the xz -plane passing through the charge group on the concave surface. We observe that the water density near the charge group is much higher compared to that in the bulk, and the heights of the density peaks are similar for water near both the concave and convex surfaces. The above results indicate that the sub-nanometer deep concave spot on the rough channel surface is hydrated well.

Figure 4b shows the effective concentration profiles of K^+ and Cl^- ions across the rough channel. We observe that the ion distribution is very different from that near a smooth surface. Specifically, two K^+ peaks, corresponding to the accumulation of K^+ ions near the concave and convex surfaces, are observed. To study how the ions screen the surface charge, we define a screen factor $S_f(z)$

$$S_f(z) = \frac{\int_0^z F(c_{K^+}(z) - c_{Cl^-}(z)) dz A_{acc,xy}}{|Q_{tot}(z)|}, \quad (3)$$

where F is the Faraday constant, $c_{K^+}(z)$ and $c_{Cl^-}(z)$ are the effective K^+ and Cl^- ion concentration at position z , respectively. $Q_{tot}(z)$ is the accumulated surface charge at position z . For the rough channel case, $Q_{tot}(z) = -2e$ if $z < 0.714$ nm, $Q_{tot}(z) = -4e$ if $z \geq 0.714$ nm. When $S_f(z)$

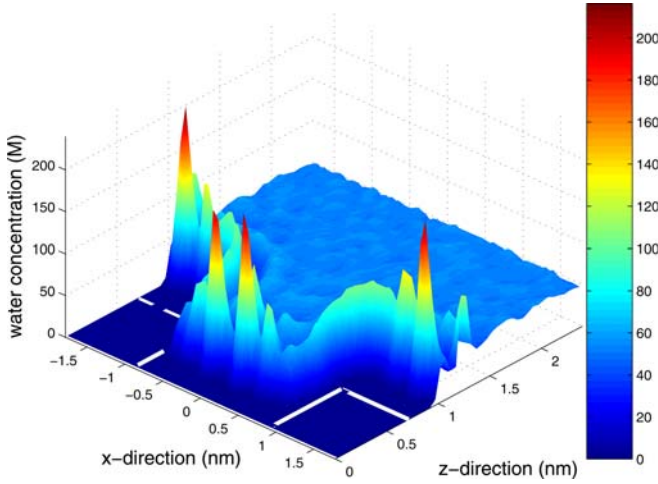


Fig. 5 Water density distribution across the rough channel surface. The *white solid lines* denote the convex solid wall surfaces (see Fig. 1b, c)

reaches 1.0, the surface charge is totally screened. Figure 6 shows the screen factor for the smooth and rough channel cases. Comparison of the screening factor in region $z < 0.714$ nm indicates that the surface charges are screened less effectively in the concave region compared to that near a smooth surface, i.e., counter-ions accumulation in the concave region is less significant compared to that near a smooth surface. To understand this, we investigate the detailed distribution of K^+ ions near the charged surface. Figure 7 shows the K^+ ion concentration distribution at the xz -plane crossing the charge group. We observe that the K^+ ion accumulates mainly near the charge groups, and its concentration near surfaces 1–2 and 3–4 are very low, i.e., it cannot access the entire volume of the concave region well. This

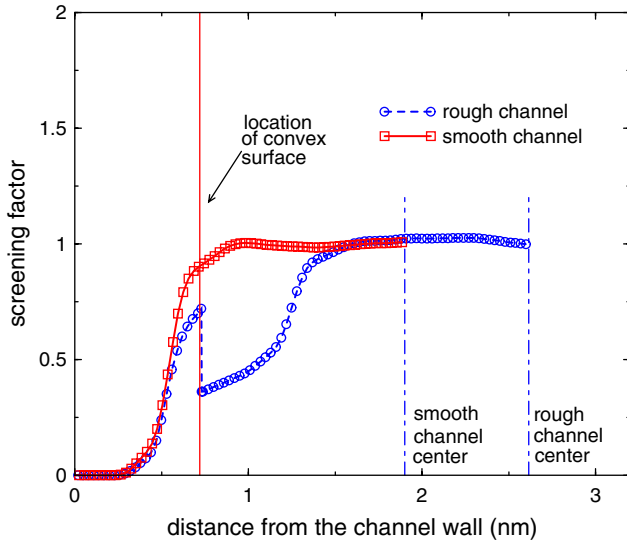


Fig. 6 Screen factor $S_f(z)$ in the smooth and rough channel cases. The sudden drop of $S_f(z)$ at $z = 0.714$ nm coincides with the introduction of charge groups at the convex surface (located at $z = 0.714$ nm)

is not surprising because a K^+ ion approaching these surfaces will lose some of its hydration water molecules, which is energetically costly. In summary, the presence of additional surfaces (surfaces 1–2 and 3–4) limits the accumulation of K^+ ions in the concave region, and this then leads to the less effective screening of the surface charges.

The electroosmotic velocity profile across the rough channel is shown in Fig. 3. We observe that, compared to the smooth channel, the electroosmotic flow is significantly reduced. The ζ -potential of the rough channel surface, computed by using Eq. 1, is found to be -13.48 mV, i.e., 36% smaller than that of the smooth surface. Such a decrease is caused by the fact that though the counter-ions in the concave regions of the rough surface can render driving force for the flow, the flow induced in the concave region is significantly retarded by the rough surface.

4 Conclusion

In summary, electroosmotic flow near smooth and rough surfaces is studied using molecular dynamics simulations. The rough surface is characterized by nanometer wide concave regions with sub-nanometer depth that is comparable to the thickness of the electrical double layer. The simulation results indicate that the ion distribution in the electrical double layer can be affected strongly by the surface roughness and the surface charge are screened less effectively in the concave region as compared to that near the smooth surface. The electroosmotic flow in the rough channel is significantly lowered compared to that in the smooth channel. Together these results indicate that the electroosmotic flow and electrical double layer can be significantly altered by the surface roughness. It would be interesting to study further how surface roughness of different

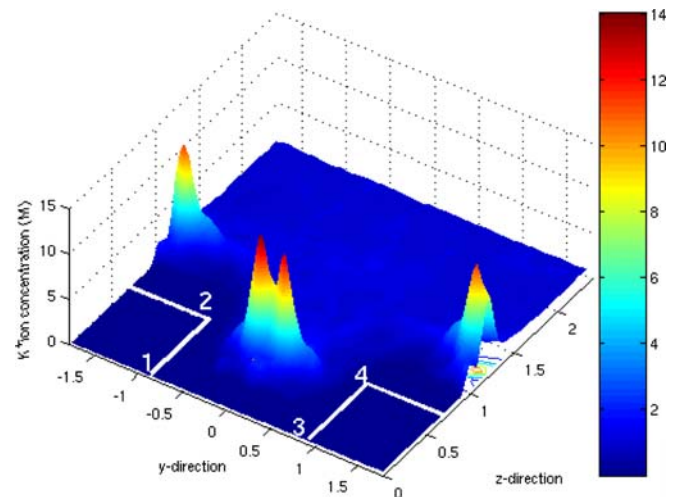


Fig. 7 K^+ ion concentration distribution near the rough channel surface. The *white solid lines* denote the convex solid wall surfaces (see Fig. 1b, c)

dimension (e.g., lateral size and depth) and pattern [e.g., symmetry vs. asymmetrical configuration (Hu et al. 2003)] will regulate the electroosmotic flow (and ζ -potential) near the surface at different electrical double layer thickness. Understanding these issues will provide valuable insights into the design of channel surfaces to achieve optimal flow control in micro- and nanofluidic systems.

References

- Berendsen HJC, Grigera JR, Straatsma TP (1987) The missing term in effective pair potentials. *J Phys Chem* 91:6269–6271
- Berendsen HJC, van der Spoel D, van Drunen R (1995) Gromacs: a message-passing parallel molecular dynamics implementation. *Comp Phys Comm* 91:43–56
- Dukhin SS, Derjaguin BV (1974) Electrikinetic phenomena. In: Matijevic E (ed) *Surface and colloid science*, vol 7. Wiley, New York
- Harrison D, Fluri K, Fan Z, Effenhauser C, Manz A (1993) Micromachining a miniaturized capillary electrophoresis-based chemical analysis system on a chip. *Science* 261:895–897
- Ho C, Qiao R, Heng JB, Chatterjee A, Timp RJ, Aluru NR, Timp G (2005) Electrolytic transport through a synthetic nanometer-diameter pore. *Proc Natl Acad Sci USA* 102:10445–10450
- Hu Y, Werner C, Li D (2003) Electrokinetic transport through rough microchannels. *Anal Chem* 75:5747–5758
- Karniadakis GE, Beskok A, Aluru NR (2005) *Microflows and nanoflows*. Springer, Berlin Heidelberg New York
- Kemery PJ, Steehler JK, Bohn PW (1998) Electric field mediated transport in nanometer diameter channels. *Langmuir* 14:2884–2889
- Koneshan S, Rasaiah JC, Lynden-Bell RM, Lee SH (1998) Solvent structure, dynamics, and ion mobility in aqueous solution at 25 C. *J Phys Chem B* 102:4193–4204
- Kuo TC, Sloan LA, Sweedler JV, Bohn PW (2001) Manipulating molecular transport through nanoporous membranes by control of electrokinetic flow: Effect of surface charge density and Debye length. *Langmuir* 17:6298–6303
- Lindahl E, Hess B, van der Spoel D (2001) Gromacs 3.0: a package for molecular simulation and trajectory analysis. *J Mol Mod* 7(8):306–317
- Lyklema J (1995) *Fundamentals of interfaces and colloid science*. Academic, San Diego
- Nose S (1984) A molecular dynamics method for simulations in the canonical ensemble. *Mol Phys* 52:255–268
- Probstein R (1994) *Physicochemical hydrodynamics*. Wiley, New York
- Qiao R, Aluru NR (2003) Ion concentrations and velocity profiles in nanochannel electroosmotic flows. *J Chem Phys* 118:4692–4701
- Qiao R, Aluru NR (2005) Atomistic simulation of KCl transport in charged silicon nanochannels: interfacial effects. *Colloids Surfaces A Physicochem Eng Aspects* 267:103–109
- Qu W, Mala GM, Li D (2000) Pressure-driven water flows in trapezoidal silicon microchannels. *Intl J Heat Mass Transfer* 43:353–364
- Santiago JG (2001) Electroosmotic flows in microchannels with finite inertial and pressure forces. *Anal Chem* 73:2353–2365
- Tessier F, Slater GW (2006) Effective debye length in closed nanoscopic systems: A competition between two length scales. *Electrophoresis* 27:686–693
- Travis KP (2000) Poiseuille flow of Lennard–Jones fluids in narrow slit pores. *J Chem Phys* 112:1984–1994
- Watzig H, Kaupp S, Graf M (2003) Inner surface properties of capillaries for electrophoresis. *Trends Anal Chem* 22:588–604
- Yang C, Li D (1997) Electrokinetic effects on pressure-driven liquid flows in rectangular microchannels. *J Colloid Interface Sci* 194:95–107
- Yeh I, Berkowitz M (1999) Ewald summation for systems with slab geometry. *J Chem Phys* 111(7):3155–3162